Hemin-based biomimetic synthesis of PANI@iron oxide and its adsorption of dyes

Huifang Xie[a], Mei Yan[a], Qing Zhang[a], Hongxia Qu[b],*, Jinming Kong[a]

[a]*Jiangsu Key Laboratory of Chemical Pollution Control and Resources Reuse, School of Environmental and Biological Engineering, Nanjing University of Science and Technology, Nanjing 210094, Jiangsu Province, China, emails: huifangxie@hotmail.com (H. Xie), 1594610692@qq.com (M. Yan), 1369447083@qq.com (Q. Zhang), j.kong@njust.edu.cn (J. Kong)*
[b]*School of Chemical Engineering, Nanjing University of Science and Technology, Nanjing 210094, Jiangsu Province, China, email: qhx@mail.njust.edu.cn*

a b s t r a c t

In this work, a polyaniline@iron oxide (PANI@iron oxide) composite was synthesized by using an eco-friendly hemin-based biomimetic method at mild conditions. The PANI@iron oxide composite was characterized with scanning electron microscopy, UV–Vis, Fourier transform infrared spectroscopy, X-ray diffraction and thermal gravimetric analysis, and its adsorption behavior was further tested. Results showed that PANI@iron oxide can efficiently remove both anionic and cationic dyes from aqueous solution. For adsorption of dyes of methyl orange (MO) and rhodamine B (RhB) on PANI@iron oxide, the kinetic data match well with pseudo-second-order model. The adsorption data were evaluated using Langmuir, Freundlich and Dubinin–Radushkevich isothermal models. For MO, high correlation coefficients (R^2) confirmed the validity of Langmuir isotherm, with monolayer adsorption capacity of 63.89 mg g^{-1}. For RhB, the Freundlich isotherm was precisely fit the equilibrium data. The values of $\Delta H°$ and $\Delta G°$ in the thermodynamic parameters indicated that the adsorption of dyes is endothermic and spontaneous. The value of $\Delta S°$ revealed that randomness at the solid–solution interface increases. NaOH solution was effective for desorption of dyes from PANI@iron oxide. For PANI, dedoping process happened during desorption, and then the structure and charge changed during desorption process.

Keywords: Biomimetic synthesis; Hemin; Polyaniline@iron oxide; Adsorption; Anionic and cationic dyes

1. Introduction

Dye removal from industrial effluents has received intense attention because of stringent environmental legislation and discharge standards. Generally, dyes are toxic, mutagenic as well as carcinogenic [1–3]. Among various methods for treating dye effluent, adsorption is one of the most effective and economic ways [4,5].

Polyaniline (PANI) is regarded as a potential adsorbent due to it exhibits remarkable surface area and porosity, good stability and low cost [1,6]. For adsorption of dyes, chemically synthesized PANI shows high selectivity. Cationic dyes can be preferentially removed by the base-treated PANI [7] while the anionic dye is predominately removed by the acid-treated one [7–9]. Effluent of dyes industries contains different kinds of dyes, so the selective adsorption limits its application in wastewater treatment. Furthermore, the direct use of PANI powder as absorbent is also limited by the fine particle size, complicated diffusion process, hard separation after adsorption and very low optimal pH values [10].

Iron oxide is an abundant material in nature and can adsorb dyes containing secondary and tertiary amines, carboxylic group, oxygen and sulfur atoms due to hydrogen bonding, van der Waal forces and others [11]. So the introduction of iron oxide in the composite can improve the application performance of PANI [12,13]. It was reported that the polyaniline/iron oxide (PANIIO) remained the selectivity of PANI for anionic dyes at low pH (2.0) [12]. The core–shell structure

* Corresponding author.

Fe$_3$O$_4$/PANI was used to adsorb DNA [13] and anionic dye, but the equilibrium adsorption capacity in near neutral solution is relatively low [14]. So new effective PANI-based adsorbents are needed for the practical utility on wastewater treatment.

As mentioned above, the most widely used synthesis methods of PANI-based absorbents now are chemical oxidative polymerization in strong acid solution. The chemical methods are rather unfavorable ecologically because the large amount of strong oxidants such as peroxydisulfate and ferric chloride are consumed [12,13,15,16]. Enzymatic oxidative polymerization catches the attention of researchers because it is a clean and eco-friendly process. Peroxidase and laccase are main enzymes related to PANI synthesis [17]. In our previous study, laccase-catalyzed preparation of polyaniline/graphene oxide composite provided an environmental benign method for the polymerization of PANI [18]. However, the drawbacks for enzyme's oxidative polymerization are obvious with its high cost, low activity, narrow pH optimum range and low stability of enzymes. So, using synthetic systems to mimic natural enzymes with high catalytic activity has attracted interest recently. Hemin is the catalytic active center of peroxidase and has been reported to catalyze a variety of oxidation reactions like peroxidase [19–21]. So hemin-based biomimetic synthesis provides an eco-friendly method for the preparation of PANI/iron oxide.

In this paper, PANI/iron oxide was prepared by hemin-catalyzed polymerization in the presence of iron oxide at mild conditions. The PANI/iron oxide showed a good adsorption capacity for both anionic and cationic dyes. The characterization of absorbent and its adsorption properties were investigated and the adsorption kinetics, isotherms and thermodynamics were studied.

2. Experimentals

2.1. Material

Aniline was purified by distilling before use. Hemin was purchased from Bioduly Co., Ltd., Nanjing, China, and stored in the dark at 4°C. Hydrogen peroxide (30% w/v; Sinopharm Chemical Reagent Co., Ltd., Shanghai, China) was used and the initial concentration was determined by titrating with standardized potassium permanganate (KMnO$_4$) solution. Methyl orange (MO) and rhodamine B (RhB) were purchased from Tianjin Chemical Reagents Co., Ltd., Tianjin, China. Other chemicals were of analytical grade.

2.2. Biomimetic synthesis of PANI@iron oxide

Iron oxide was synthesized by co-precipitation method. Typically, 1 M ferrous sulfate and 2 M ferric chloride were dissolved into 0.01 M HCl solution, then the mixture was slowly dropped into 250 mL of 1.5 M aqueous sodium hydroxide under continuous stirring at 60°C and the reaction was carried out for 30 min. The black power obtained was washed sequentially with water and ethanol and then was dried at 60°C. The formation of maghemite (iron oxide) was confirmed by X-ray diffraction (XRD).

For biomimetic synthesis of PANI@iron oxide, 0.05 M aniline, 0.01 g·L^{-1} hemin and 2.5 g·L^{-1} iron oxide were added into sodium citrate–citric acid buffer solution (pH = 4.00). Then 0.2 mL 0.06 M H$_2$O$_2$ was injected every 15 min. After total

1.4 mL H$_2$O$_2$ solution was added, the polymerization proceeded for 0.5 h at room temperature. Then 25 mL of 37% HCl was added and the mixture was kept stirring for 0.5 h, and was placed at room temperature for 16 h. The formed PANI@iron oxide was collected via centrifugation at 3,500 rpm and washed sequentially with water and ethanol and the washed PANI@iron oxide was dried at 60°C.

2.3. Characterization of PANI@iron oxide

The morphological feature was collected by field emission scanning electron microscopy (FE-SEM, FEI Quanta 250FEG) at high voltage of 30 kV and Fourier transform infrared (FT-IR) spectrum was recorded with an FT-IR spectrometer (PerkinElmer FT-IR spectrophotometer CA, USA). XRD patterns were recorded on a Bruker D8 Advance diffractometer.

PANI and PANI@iron oxide were dissolved in *N*-methylpyrrolidone, respectively, and UV–Vis spectra were recorded by UV–Vis spectrophotometer (Lambda 25, PerkinElmer, USA). Thermal gravimetric analysis (TGA) curves were recorded on a TGA/SDTA 851e diffractometer. Surface area and pore size were determined with an ASAP 2020 surface area and porosity analyzer (Micromeritics, USA).

2.4. Adsorption experiments

Batch adsorptions were performed by shaking (150 rpm) 50 mg PANI@iron oxide in 100 mL different initial concentrations (10–50 mg·L^{-1}) of dye solution at a fixed temperature (25°C–55°C) in a shaker bath for 3 h. For each adsorption experiment, the supernatant was filtrated with syringe filter at certain intervals and analyzed. Removal ratio (%) and adsorption capacity Q (mg·g^{-1}) were calculated according to the following equations:

$$\text{Removal ratio} = \frac{(C_0 - C_t)}{C_0} \times 100\% \qquad (1)$$

$$Q = \frac{V(C_0 - C_t)}{m} \qquad (2)$$

where C_0 and C_t are the concentrations of dyes (mg·L^{-1}) initially and at time t, V is the volume of solution (L) and m is the mass of PANI@iron oxide used (g).

The experiments were performed in triplicate for all the operating variables studied. The mean and standard deviation of the removal ratio were determined. For adsorption kinetics and isotherms, only the average values were considered.

2.5. Desorption and recycling experiments

The dyes loaded adsorbent was treated with 100 mL of 0.1 M NaOH or HCl solution for desorption. After equilibrating, the mixture was filtered and the filtrate was analyzed. The desorption ratio D (%) was calculated using Eq. (3):

$$D = \frac{m_{de}}{m_{da}} \times 100\% \qquad (3)$$

where m_{da} is the mass of dye adsorbed on adsorbent and m_{de} is the mass of dye returned into solution at desorption equilibrium time.

At the same time, the adsorbent was washed with water and dried at 60°C for reuse. The adsorption–desorption processes were carried out for three times.

3. Results and discussion

3.1. Characterization of PANI@iron oxide

The morphologies of the synthesized PANI@iron oxide were investigated by scanning electron microscopy (SEM). The typical micrographs are presented in Fig. 1(A). It is evident that the composites are irregular fine granules from 0.5 to 50 μm with rough surface and pleats. The BET surface area is 22.9 $m^2 \cdot g^{-1}$ and the BET average pore width is 10.9 nm. The size and surface can provide good possibilities to trap and adsorb dyes.

In UV–vis spectra (Fig. 1(B)) of PANI and PANI@iron oxide, the absorption band at 354 nm are attributed to $\pi \rightarrow \pi^*$ transitions in the benzene ring and the shoulder at 590 nm
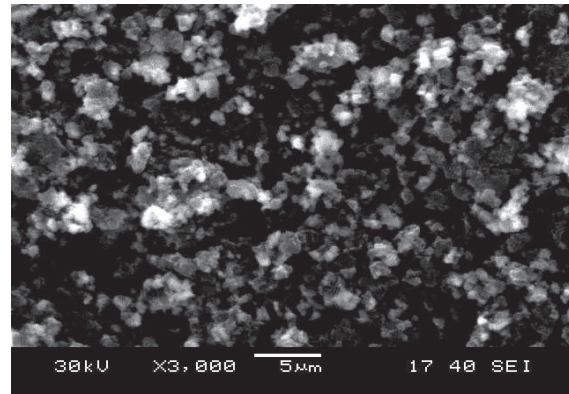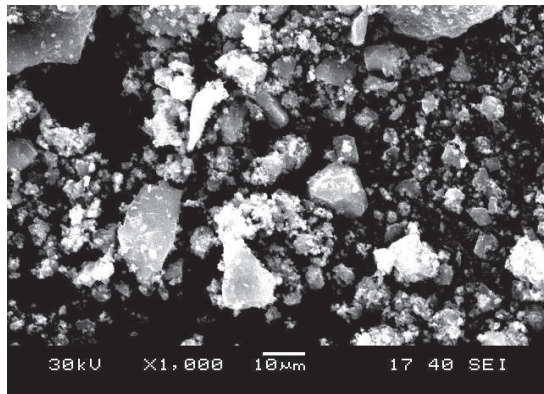
A. SEM images of PANI@iron oxide
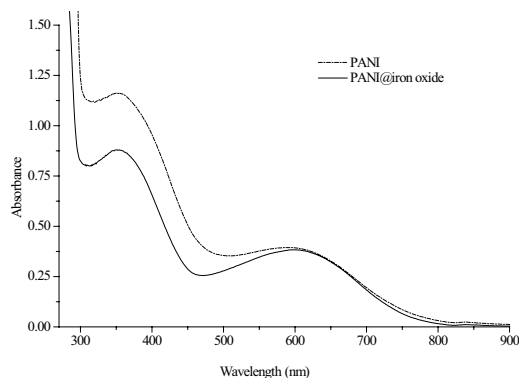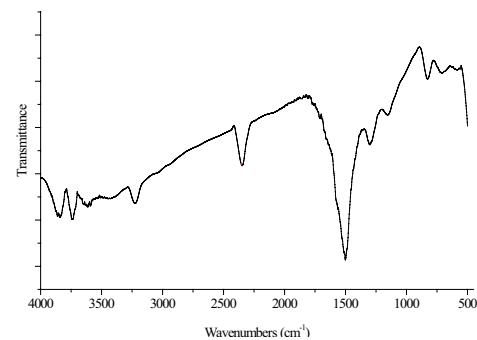
B. Uv-vis spectra of PANI and PANI@iron oxide

C. FT-IR spectrum of PANI@iron oxide
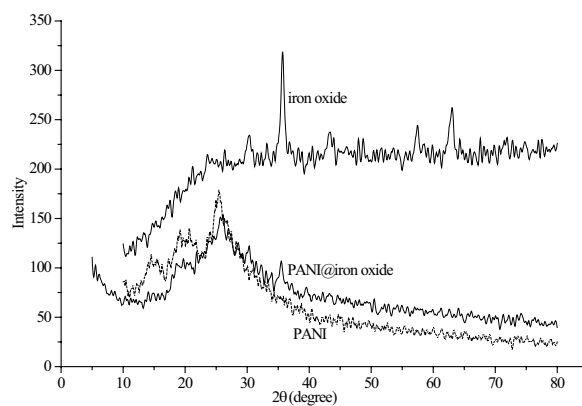
D. XRD patterns of PANI, iron oxide and PANI@iron oxide
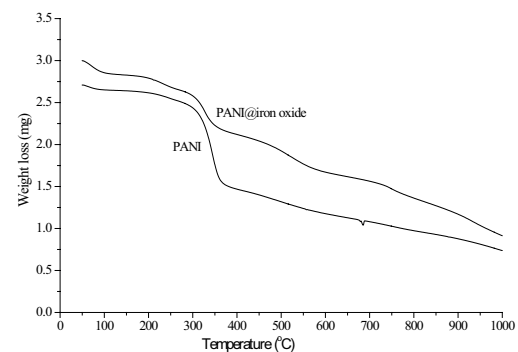
E. TGA of PANI and PANI@iron oxide

Fig. 1. SEM, UV–Vis spectra, FT-IR spectrum, XRD patters and TGA curves: (A) SEM images of PANI@iron oxide, (B) UV–Vis spectra of PANI and PANI@iron oxide, (C) FT-IR spectrum of PANI@iron oxide, (D) XRD patterns of PANI, iron oxide and PANI@iron oxide, (E) TGA of PANI and PANI@iron oxide.

to the benzene to quinoid ring excitonic transition [22,23]. Compared with the band at 354 nm in pure PANI, the band in PANI@iron oxide is weaker. It is well-known that the position of this peak is sensitive to the nature of the counter ions and solvent and to the chemical structure of the polymer [24]. In this case, the observed weak peak is associated with the latter factor, which indicates the interaction between PANI and iron oxide.

The FT-IR spectrum of the PANI@iron oxide is shown in Fig. 1(C). Peaks observed at 2,359, 1,506, 1,290, 1,147 and 827 cm^{-1} can be assigned to N–H bending, benzenoid or quinonoid C=C, C–N bending, C–H in-plane bending and C–H and/or N–H out-of-plane bending vibrations in PANI, respectively. The weak peak during 540–700 cm^{-1} corresponds to Fe–O vibration [13,25–28]. The spectrum is featured with dramatical sloping line at wave numbers higher than 2,000 cm^{-1}, which signals the conducting form of PANI [24,29]. The peaks at 1,506, 1,290 and 1,147 cm^{-1} redshift in peak position as compared with the peaks at 1,585.71, 1,298.98 and 1,150.89 cm^{-1} in PANIIO chemically synthesized [12]. The results indicate that the increase of delocalization in PANI@iron oxide synthesized in hemin-based biomimetic method. More compact combination of iron oxide and N in PANI strengthens the corresponding C–N bond due to donation of electrons from benzenoid or quinonoid rings, and concurrently weakens the bond strength of C=C, N–H and C–H.

The XRD patterns of PANI, iron oxide and PANI@iron oxide are shown in Fig. 1(D). The Bragg diffraction peaks of $2\theta = $ ~15.5°, ~20.7° and 25.4° can be found in PANI, which shows that PANI has a partly crystalline structure. The peaks in PANI prepared by hemin-catalyzed polymerization are similar to that in PANI by chemical oxidation [30,31]. The two characteristic peaks of PANI salts, which centered $2\theta = 20°$ and 25°, are remained in PANI@iron oxide with weaker summit and broader range comparing with those in pure PANI [31,32]. The changes indicate that main structure of PANI retains, but the crystalline is distorted during the polymerization in the presence of iron oxide. At the same time, the peaks at $2\theta = 30.3°, 35.6°, 43.3°$ and 63.0° show the characteristics of maghemite in PANI@iron oxide pattern, but decrease in intensity due to PANI coating. The decrease in intensity is also found in other PANI and Fe$_3$O$_4$ composites synthesized by chemical oxidation [13,14].

From Fig. 1(E), the mass loss below 100°C is attributed to the deintercalation of water. The TGA curves for PANI show a two-step weight loss because of the elimination of the doped acid bound to PANI chains (200°C–350°C) and decomposition of the pristine PANI backbone (>350°C), respectively [32,33]. The TGA curve of PANI@iron oxide shows similar weight loss step, while the mass loss is lower than that of PANI. This lower mass loss is in accordance with previous reports when an inorganic oxide was introduced into PANI-based composite [32,33].

It can be concluded from the above characteristics of PANI@iron oxide that the PANI coat on the surface of iron oxide is partly in PANI@iron oxide and there is a compact combination between polymer and iron oxide. The partly coating of PANI on iron oxide particles can protect iron oxide from leaching and remain functional groups of PANI and iron oxide.

3.2. Adsorption for anionic and cationic dyes

The primary adsorption study on dyes removal by PANI@iron oxide was carried out on anionic (MO) and cationic (RhB) dyes, and the removal profiles are shown in Fig. 2. The adsorption removal ratios of two dyes increase with contact time and there is an initial rapid phase and a slower phase for adsorption removal. The optimized contact time is selected as 120 min. MO is removed 55.4% in 10 min and 94.0% in 120 min by PANI@iron oxide. It should be noted that the PANI@iron oxide can remove 41.4% in 10 min and 66.5% in 120 min RhB from solution, respectively. The facts prove that PANI@iron oxide can remove both anionic and cationic dyes effectively.

It has been reported that chemically synthesized PANI and PANI/iron oxide had no adsorption for cationic dyes [8,9,12]. In contrast, our results showed that the biomimetic synthesized PANI@iron oxide can adsorb cationic dyes RhB. The capacity of RhB on PANI@iron oxide is about 35 mg g^{-1}. This adsorption capacity is much higher than that of some reported absorbent, such as natural materials [3,5,34], fly ash [11] and is comparable with that of kaolinite [4] and biomass of *Rhizopus oryzae* [35].

That is to say, as-prepared PANI@iron oxide has wider adsorption range for dyes. However, the removal ratio of MO is much higher than that of RhB, so the adsorption behaviors of MO are analyzed in detail. The results of RhB adsorption are presented in Supporting information. The possible reason is that the PANI@iron oxide contains more abundant adsorption sites of amine, imine (PANI) and –OH (iron oxide). Compared with chemical polymerization of PANI [7], the synthesis conditions are mild in hemin/H$_2$O$_2$ system. There are at least four idealized forms of PANI, emeraldine salt, emeraldine base, leuco salt and leuco base according to the synthesis condition and subsequent treatment [7]. This biomimetic synthesized product might be the mixture of different doping level forms of PANI and iron oxide. For anionic dye, MO, the electrostatic interaction between the anionic sulfonic groups and the positive charged N in PANI is the main force of adsorption; for cationic dye, RhB, the hydrophobic interaction and hydrogen bonding play the roles.
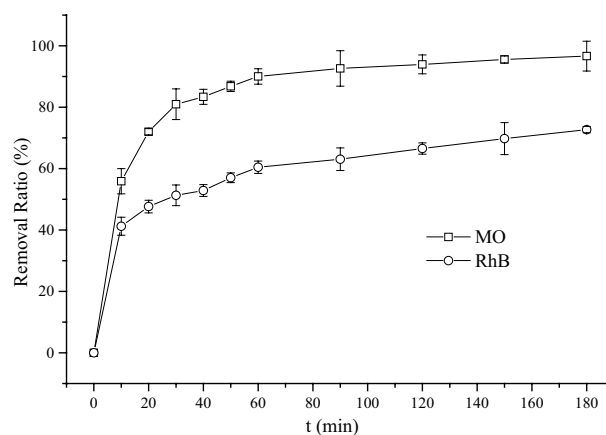
Fig. 2. Removal profile of MO and RhB. Initial concentrations of dyes 20 mg L^{-1}, temperature 25°C, PANI@iron oxide dosage 0.5 g L^{-1}, without pH adjustment.

3.3. Adsorption kinetics

The pseudo-second-order model is given by Eq. (4):

$$\frac{t}{Q_t} = \frac{1}{k_2 Q_e^2} + \frac{1}{Q_e} t \tag{4}$$

where Q_e and Q_t (mg·g⁻¹) are the amounts of dye adsorbed at equilibrium and time t (min), respectively. k_2 (g·mg⁻¹·min⁻¹) is the order rate constant. The plot t/Q_t vs. t at different initial MO is shown in Fig. 3 and the values of Q_e, k_2 and the correlation coefficients are summarized in Table 1.

At all studied initial dye concentrations, the straight lines with extremely high correlation coefficients (≥0.997) were obtained. The results suggest that the adsorption of MO onto PANI@iron oxide is governed by pseudo-second-order rate kinetics. The rate constant is much bigger than that of some reported adsorbent followed the pseudo-second-order kinetics, such as nanoparticle Fe₃O₄/PANI [14] and hyper-cross-linked polymer [36] (see Table 2). From the point of the adsorption rate, PANI@iron oxide is a kind of ideal adsorbent.

Similarly, the adsorption of RhB onto PANI@iron oxide is also governed by pseudo-second-order rate kinetics (see Supporting information).

3.4. Adsorption isotherms

Three isotherm models (Langmuir, Freundlich and Dubinin–Radushkevich (D–R)) were applied to describe adsorption and the equations are as follows:
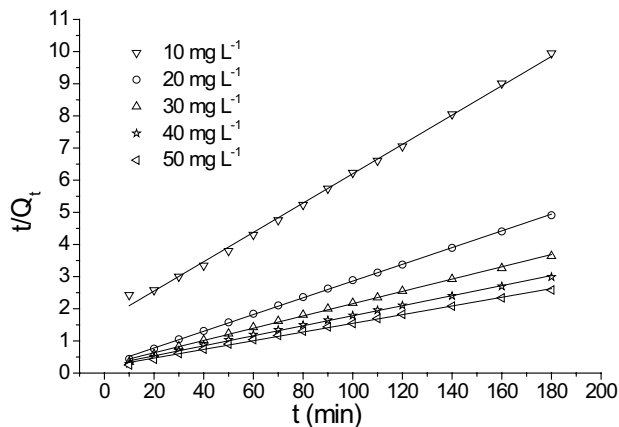
Fig. 3. Pseudo-second-order kinetic plots at different MO concentrations at 25°C.

Table 1
Adsorption kinetic parameters of MO

MO (mg·L⁻¹)	Q_e (mg·g⁻¹)	k_2 (×10⁻³) (g·mg⁻¹·min⁻¹)	R^2
10	21.93	1.27	0.9975
20	39.97	2.61	0.9995
30	52.38	1.46	0.9983
40	64.14	1.08	0.9980
50	64.47	0.93	0.9977

Langmuir:

$$\frac{C_e}{Q_e} = \frac{1}{Q_{max} \cdot K_L} + \frac{C_e}{Q_{max}} \tag{5}$$

Freundlich:

$$\ln Q_e = \ln K_F + \frac{1}{n} \cdot \ln C_e \tag{6}$$

D–R:

$$\ln Q_e = \ln Q_{max} - K_{DR} \cdot \varepsilon^2 \tag{7}$$

where Q_{max} is the maximum adsorption capacity (mg·g⁻¹), K_L is the Langmuir constant (L·mg⁻¹) and C_e (mg·L⁻¹) is the equilibrium concentration of MO in solution. K_F is the Freundlich constant. K_{DR} (mol²·kJ⁻²) is the D–R model constant. ε is the Polanyi potential, which is related to the equilibrium concentration using Eq. (8):

$$\varepsilon = RT\ln\left(1 + \frac{1}{C_e}\right) \tag{8}$$

where R is the ideal gas constant (8.314 J·K⁻¹·mol⁻¹) and T is the absolute temperature (K). The constant K_{DR} gives the mean free energy E (kJ·mol⁻¹). E can be calculated using the Eq. (9) [37]:

$$E = \frac{1}{\sqrt{2K_{DR}}} \tag{9}$$

By comparing the correlation coefficients of three models in Table 3, it is concluded that the adsorption data followed the Langmuir isotherm model at temperature 25°C–55°C. Langmuir isotherm is valid for monolayer adsorption, so the fitting indicates the monolayer coverage of MO on the surface of PANI@iron oxide. The results are similar to the adsorption of MO on nanoparticle Fe₃O₄/PANI and Fe₃O₄. The value of n in Freundlich isotherm is greater than 1, which indicates that the MO is favorably adsorbed onto PANI@iron oxide. The values of E in D–R model are 2.89–3.03 kJ·mol⁻¹. It is reported that when E is less than 8 kJ·mol⁻¹, the process follows physical adsorption [38]. Therefore, the adsorption of MO on PANI@iron oxide can be mainly considered to be influenced by physical force.

As far as RhB is concerned, the Freundlich isotherm model was precisely fit the equilibrium data at temperature ranging from 298 to 328 K. And the values of n are greater than 1, which also indicate that the RhB is favorably adsorbed onto PANI@iron oxide (see Supporting information).

3.5. Adsorption thermodynamics

Gibbs free energy ($\Delta G°$) is the fundamental criterion of spontaneity of a process and can be determined by Eq. (10):

$$\Delta G° = -RT\ln K \tag{10}$$

Table 2
Comparison of MO adsorption with some reported adsorbent

Absorbents	Kinetics	Isotherms	Thermodynamics	Capacity (mg g^{-1})	Reference
PANI@iron oxide	Pseudo-second-order: $k_2 = 1.08 \times 10^{-3}$ g mg^{-1}·min^{-1} ($T = 298$ K)	Langmuir: $K_L = 1.089$ L mg^{-1} ($T = 298$ K)	Spontaneous: $\Delta H = 10.51$ kJ mol^{-1}, endothermic	63.89	This study
Activated carbon	Pseudo-first-order: $k_1 = 9.68 \times 10^{-3}$ ($T = 303$ K)	Freundlich: $K_F = 0.0013$ mol g^{-1}, $1/n = 0.3761$ ($T = 303$ K)	Spontaneous: $\Delta H = 82.15$ kJ mol^{-1}, endothermic	9.41	[40]
Banana peels	Pseudo-first-order: $k_1 = 0.39$ min^{-1}; intraparticle diffusion: $K_p = 2.42$ mg g^{-1}·min$^{-1/2}$	Freundlich: $K_F = 1.73$ mg g^{-1}, $1/n = 2.20$ ($T = 303$ K)		21	[34]
Orange peels	Pseudo-first-order: $k_1 = 0.4$ min^{-1}; intraparticle diffusion: $K_p = 1.68$ mg g^{-1}·min$^{-1/2}$	Freundlich: $K_F = 0.26$ mg g^{-1}, $1/n = 0.17$ ($T = 303$ K)		20.5	[34]
Hyper-cross-linked polymer	Pseudo-second-order: $k_2 = 1.82 \times 10^{-5}$ g mg^{-1}·min^{-1} ($T = 293$ K)	Freundlich: $K_F = 5.4075$ L mg^{-1}, $n = 2.15$ ($T = 293$ K)	Spontaneous: $\Delta H = -24.28$ kJ mol^{-1}, exothermic	70.92	[36]
Nanoparticle Fe$_3$O$_4$/PANI	Pseudo-second-order: $k_2 = 3.91 \times 10^{-4}$ g mg^{-1}·min^{-1} ($T = 298$ K)	Langmuir: $K_1 = 2.33$ L mg^{-1} ($T = 288$ K)		105.8	[14]
Fe$_3$O$_4$		Langmuir: $K_1 = 3.25$ L mg^{-1} ($T = 288$ K)		2.38	[14]

Table 3
Fitting parameters for MO adsorption on PANI@iron oxide based on isotherm models

T (K)	Q (mg·g^{-1}) (experimental value)	Langmuir			Freundlich			D–R		
		Q_{max} (mg·g^{-1})	K_L	R^2	K_F	R^2	n	K_{DR} ($\times 10^{-8}$)	E (kJ·mol^{-1})	R^2
298	63.89	64.14	1.089	0.9972	31.42	0.9581	3.693	5.69	2.96	0.9406
308	58.78	61.61	1.365	0.9977	30.31	0.9313	3.939	5.45	3.03	0.9632
318	59.28	60.50	1.445	0.9977	30.46	0.9478	3.801	5.98	2.89	0.9452
328	61.52	64.27	1.634	0.9980	33.41	0.9814	2.980	5.86	2.92	0.8928

Enthalpy change ($\Delta H°$) and entropy change ($\Delta S°$) are calculated by Eq. (11):

$$\ln K = \frac{\Delta S°}{R} - \frac{\Delta H°}{RT} \tag{11}$$

Here $K = Q_e/C_e$ is the distribution coefficient.

According to the linear plot of $\ln K$ vs. $1/T$, $\Delta G°$, $\Delta H°$ and $\Delta S°$ were calculated and the results are shown in Table 4.

The positive value of $\Delta H°$ shows that the adsorption of MO on PANI@iron oxide is endothermic in nature. Similar findings were observed during the adsorption of AB10B onto a composite of PANIIO [12]. It has been reported that $\Delta H°$ for a physical adsorption rarely exceed 16.75 kJ·mol^{-1} [39], so this value implies that the nature of MO adsorption is a physical adsorption. The result is in accord with that in D–R isotherm model analysis. But the $\Delta H°$ of RhB adsorption is a little higher (see Supporting information), which indicates there are different adsorption forces from MO adsorption on the PANI@iron oxide.

Table 4
Thermodynamic parameters for the adsorption of MO at different temperatures

T (K)	K	$\Delta G°$ (kJ·mol^{-1})	$\Delta S°$ (J·K^{-1}·mol^{-1})	$\Delta H°$ (kJ·mol^{-1})
298	1.09	−17.33	93.68	10.51
308	1.36	−18.48		
318	1.45	−19.24		
328	1.64	−20.19		

For MO and RhB adsorption, the positive value of $\Delta S°$ reveals the increasing randomness at the solid–solution interface during the adsorption process. The values of $\Delta G°$ are negative and decrease with an increase in temperature, which indicate that the adsorption process is spontaneous.

A comparison of characteristics in the present study with some reported adsorbent for MO removal is summarized in Table 2. The capacity of PANI@iron oxide is much

higher than that of some kinds of natural adsorbent [34,40] and Fe_3O_4 [14], and is similar to that of the hypercross-linked polymer [36]. In general, as-prepared PANI@iron oxide is a potential adsorbent.

3.6. Desorption and recycling use

HCl and NaOH solution were used for desorption in this study. As shown in Fig. 4, over 95% MO is released from adsorbent after 60 min in 0.1 M NaOH solution, but only 17.3% of MO desorption is achieved when 0.1 M HCl solution is used.

Three cycles of adsorption and desorption for MO were tested to assess the reusability of PANI@iron oxide. The results are shown in Fig. 5. The removal ratio of MO decreased by 14.0% and 26.8% at second and third round adsorption, respectively.

3.7. Adsorption and desorption mechanism

The FI-IR spectrum and XRD curve after adsorption of MO on PANI@iron oxide is shown in Fig. 6. The new or overlapped peaks in FT-IR after adsorption at 1,578, 1,305 and 1,140 cm^{-1} can be assigned to the MO adsorbed on the PANI@ iron oxide. After desorption by NaOH, the peaks related to MO disappear or become much weaker, which indicate that adsorbed MO return into solution from the surfaces of absorbent. The adsorption of MO seldom alerts the crystalline nature of the PANI@iron oxide, which is illustrated from the curves before and after adsorption in Figs. 1(D) and 6(B). However, the structure of PANI@iron oxide changes obviously after three cycles, just as shown in the curves of XRD in Fig. 6(B).

The structure of dye and the surface properties of adsorbent can influence the adsorption process. In acid medium, PANI chains can be protonated or oxidized and acquire positive charges localized over the polymeric backbone [7,29,41]. The counter ion, Cl$^-$, is attracted near the backbone to ensure overall charge neutrality of PANI [42]. During synthesis of PANI@iron oxide, the PANI is from partially to fully protonated form. When the composite was added into the MO solution, pH decreased dramatically from 5.89 to 2.96 and maintained stable afterward because H$^+$ is partly released into solution, as shown in Fig. 7. So, the –SO$_3$H in MO is present in the form of anion, –SO$_3^-$, and the electrostatic interaction between –SO$_3^-$ and the positively charged amine, imine and hydroxyl groups of the adsorbent can take place quickly, as shown in Fig. 8. The electrostatic force becomes the main role for adsorption of MO on PANI@iron oxide, so the removal ratio of MO is much higher than that of RhB.

Desorption with NaOH is the dedoping process for PANI and makes PANI discharged, so the electrostatic interaction
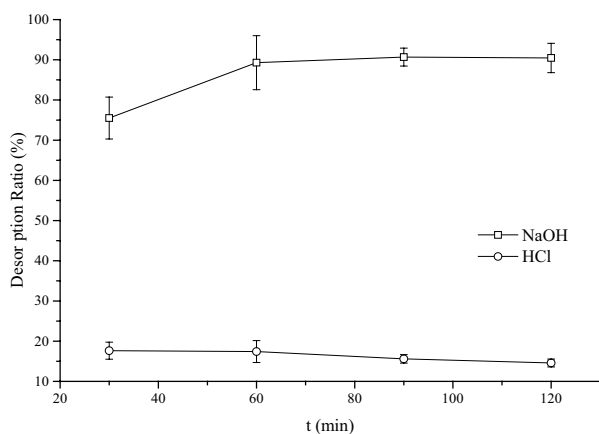
Fig. 4. Desorption profile of MO in NaOH and HCl solution.
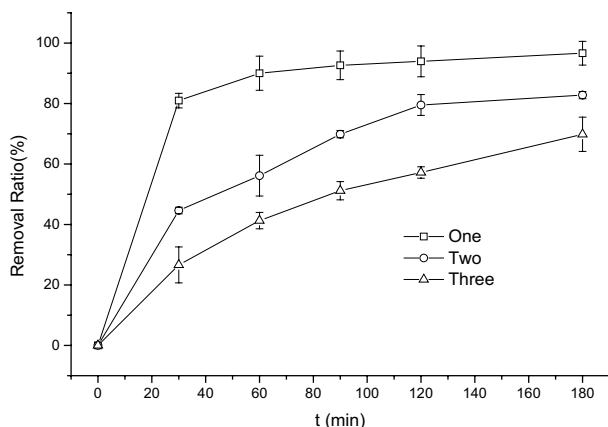
Fig. 5. Cycling performance of MO adsorption on PANI@iron oxide.
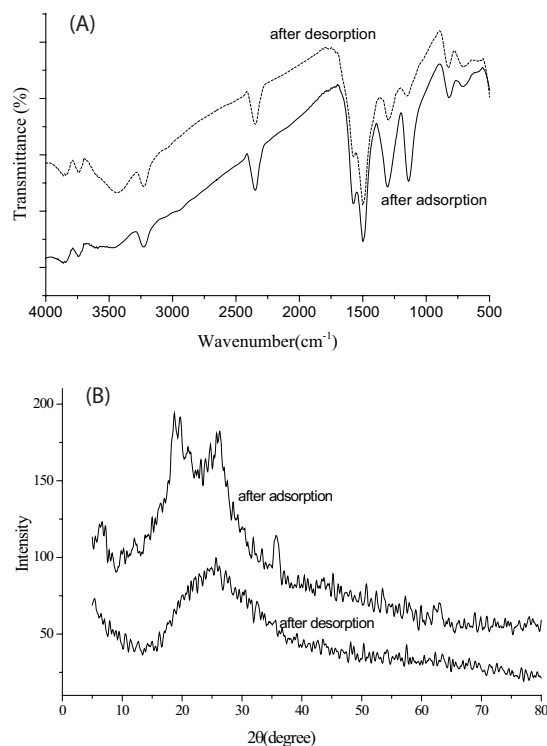
Fig. 6. FT-IR spectra (A) and XRD curves (B) after adsorption and desorption.
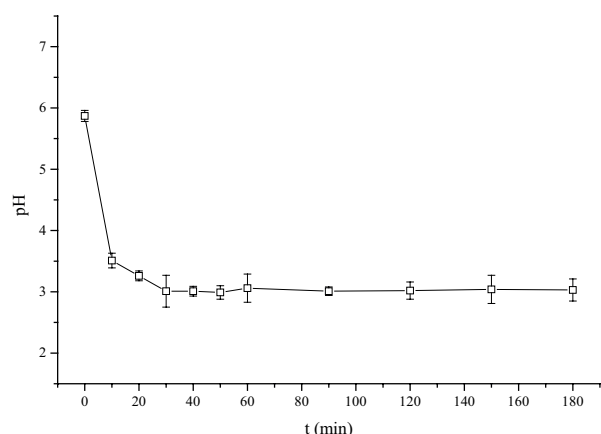
Fig. 7. pH profile during the adsorption of MO.
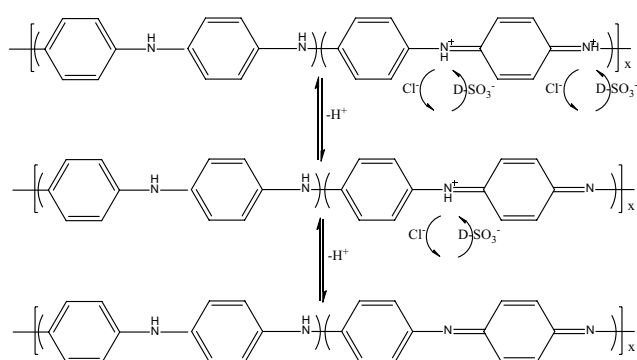
Fig. 8. The reaction of PANI during adsorption and desorption.

decreases until disappears, and MO can be released from the surface of PANI@iron oxide. It is concluded that the changes of structure and charges after desorption make the adsorption capacity decrease when PANI@iron oxide is reused. Chowdhury et al. [7] found that the acid-treated PANI matrix has the greatest adsorption capacity for the anionic dye Procion red, and base-treated PANI matrix has relatively fewer capacities. Wang et al. [14] also reported that the dedoped Fe_3O_4/PANI with ammonia water decreased adsorption capacity for MO dramatically comparing to that of Fe_3O_4/PANI prepared in acid mediums. So the decreased adsorption capacity of PANI lies in the dedoping process caused by NaOH treatment (see Fig. 8). So it is necessary to find new ways to desorb the adsorbed dyes or to regenerate the adsorbent. Our recent study showed that the alcohol–water system can be selected as desorbent.

4. Conclusion

PANI@iron oxide was synthesized at mild conditions in biomimetic hemin/H_2O_2 system, and it can adsorb both anionic and cationic dyes in aqueous solution. The adsorption behaviors for dyes of MO and RhB indicated that the pseudo-second-order kinetics rate equation were suitable to depict the adsorption kinetics. The Langmuir isotherm and Freundlich isotherm can characterize the adsorption of MO and RhB on PANI@iron oxide, respectively. The values of

$\Delta H°$ and $\Delta G°$ show that the adsorption is endothermic and spontaneous and the $\Delta S°$ reveals that randomness at the solid–solution interface increases.

The electrostatic interaction between the anionic sulfonic groups of the dye and positively charged groups of adsorbent is the main force for anionic dye, while hydrophobic interaction and hydrogen bonding make it possible for adsorption of cationic dye.

References

[1] L. Ai, J. Jiang, R. Zhang, Uniform polyaniline microspheres: a novel adsorbent for dye removal from aqueous solution, Synth. Met., 160 (2010) 762–767.
[2] M.M. Lakouraj, R.S. Norouzian, S. Balo, Preparation and cationic dye adsorption of novel Fe_3O_4 supermagnetic/thiacalix[4] arene tetrasulfonate self-doped/polyaniline nanocomposite: kinetics, isotherms, and thermodynamic study, J. Chem. Eng. Data, 60 (2015) 2262–2272.
[3] T.A. Khan, S. Sharma, I. Ali, Adsorption of Rhodamine B dye from aqueous solution onto acid activated mango (*Magnifera indica*) leaf powder: equilibrium, kinetic and thermodynamic studies, J. Toxicol. Environ. Health Sci., 3 (2011) 286–297.
[4] T.A. Khan, S. Dahiya, I. Ali, Use of kaolinite as adsorbent: equilibrium, dynamics and thermodynamic studies on the adsorption of Rhodamine B from aqueous solution, Appl. Clay Sci., 69 (2012) 58–66.
[5] T.A. Khan, N. Momina, E.A. Khan, Adsorptive removal of rhodamine B from textile wastewater using water chestnut (*Trapa natans L.*) peel: adsorption dynamics and kinetic studies, Toxicol. Environ. Chem., 95 (2013) 919–931.
[6] A.N. Chowdhury, M.A. Yousuf, M.M. Rahman, A.Q.M.Q. Hassan, In situ preparation of polyaniline/silica composites and study of their adsorption characteristics, Indian J. Chem., 41A (2002) 1562–1568.
[7] A.N. Chowdhury, S.R. Jesmeen, M.M. Hossain, Removal of dyes from water by conducting polymeric adsorbent, Polym. Adv. Technol., 15 (2004) 633–638.
[8] D. Mahanta, G. Madras, S. Radhakrishnan, S. Patil, Adsorption of sulfonated dyes by polyaniline emeraldine salt and its kinetics, J. Phys. Chem. B, 112 (2008) 10153–10157.
[9] D. Mahanta, G. Madras, S. Radhakrishnan, S. Patil, Adsorption and desorption kinetics of anionic dyes on doped polyaniline, J. Phys. Chem. B, 113 (2009) 2293–2299.
[10] M.A. Salem, The role of polyaniline salts in the removal of direct blue 78 from aqueous solution: a kinetic study, React. Funct. Polym., 70 (2010) 707–714.
[11] T.A. Khan, I. Ali, V.V. Singh, S. Sharma, Utilization of fly ash as low-cost adsorbent for the removal of methylene blue, malachite green and rhodamine B dyes from textile wastewater, J. Environ. Prot. Sci., 3 (2009) 11–22.
[12] R. Ahmad, R. Kumar, Conducting polyaniline/iron oxide composite: a novel adsorbent for the removal of amido black 10B, J. Chem. Eng. Data, 55 (2010) 3489–3493.
[13] G. Ligang, H. Xiaoyun, H. Yunhua, C. Jing, J. Haihui, C. Xincheng, Surfactant-free synthesis of Fe_3O_4@PANI and Fe_3O_4@PPy microspheres as adsorbents for isolation of PCR-ready DNA, Dalton Trans., 42 (2013) 1820–1826.
[14] Y. Wang, L. Gai, W. Ma, H. Jiang, X. Peng, L. Zhao, Ultrasound-assisted catalytic degradation of methyl orange with Fe_3O_4/polyaniline in near neutral solution, Ind. Eng. Chem. Res., 54 (2015) 2279–2289.
[15] M. Karthikeyan, K.K. Satheeshkumar, K.P. Elango, Defluoridation of water via doping of polyanilines, J. Hazard. Mater., 163 (2009) 1026–1032.

[16] G.V. Otrokhov, O.V. Morozova, I.S. Vasil'eva, G.P. Shumakovich, E.A. Zaitseva, M.E. Khlupova, A.I. Yaropolov, Biocatalytic synthesis of conducting polymers and prospects for its application, Biochemistry (Moscow), 78 (2013) 1539–1553.

[17] P. Walde, Z.W. Guo, Enzyme-catalyzed chemical structure-controlling template polymerization, Soft Matter, 7 (2011) 316–331.

[18] J. Hui, X. Jiang, H. Xie, D. Chen, J. Shen, X. Sun, W. Han, J. Li, L. Wang, Laccase-catalyzed electrochemical fabrication of polyaniline/graphene oxide composite onto graphite felt electrode and its application in bioelectrochemical system, Electrochim. Acta, 190 (2016) 16–24.

[19] J. Kong, X. Yu, W. Hu, Q. Hu, S. Shui, L. Li, X. Han, H. Xie, X. Zhang, T. Wang, A biomimetic enzyme modified electrode for H_2O_2 highly sensitive detection, Analyst, 140 (2015) 7792–7798.

[20] Y. Yao, Y. Mao, Q. Huang, L. Wang, Z. Huang, W. Lu, W. Chen, Enhanced decomposition of dyes by hemin-ACF with significant improvement in pH tolerance and stability, J. Hazard. Mater., 264 (2014) 323–331.

[21] M. Yan, H. Xie, Q. Zhang, H. Qu, J. Shen, J. Kong, Hemin based biomimetic oxidative degradation of Acid Orange 7, J. Mater. Sci. Chem. Eng., 4 (2016) 26–34.

[22] Y. Xia, J.M. Wiesinger, A.G. Macdiarmid, A.J. Epstein, Camphorsulfonic acid fully doped polyaniline emeraldine salt: conformations in different solvents studied by an ultraviolet/visible/near-infrared spectroscopic method, Chem. Mater., 7 (1995) 443–445.

[23] P. Rannou, A. Gawlicka, D. Berner, A. Adam Pron, M. Nechtschein, D. Djurado, Spectroscopic, structural and transport properties of conductive polyaniline processed from fluorinated alcohols, Macromolecule, 31 (1998) 3007–3015.

[24] J. Stejskal, M. Trchová, J. Prokeš, I. Sapurina, Brominated polyaniline, Chem. Mater., 13 (2001) 4083–4086.

[25] J.C. Medina-Llamas, A.E. Chávez-Guajardo, C.A.S. Andrade, K.G.B. Alves, C.P.D. Melo, Use of magnetic polyaniline/maghemite nanocomposite for DNA retrieval from aqueous solutions, J. Colloid Interface Sci., 434 (2014) 167–174.

[26] K. Singh, A. Ohlan, R.K. Kotnala, A.K. Bakhshi, S.K. Dhawan, Dielectric and magnetic properties of conducting ferromagnetic composite of polyaniline with γ-Fe_2O_3 nanoparticles, Mater. Chem. Phys., 112 (2008) 651–658.

[27] H. Gu, S. Tadakamalla, Y. Huang, H.A. Colorado, Z. Luo, N. Haldolaarachchige, D.P. Young, S. Wei, Z. Guo, Polyaniline stabilized magnetite nanoparticle reinforced epoxy nanocomposites, ACS Appl. Mater. Interfaces, 4 (2012) 5613–5624.

[28] Z.G. Wang, Q. Liu, B.Q. Ding, Shape-controlled nanofabrication of conducting polymer on planar DNA templates, Chem. Mater., 26 (2014) 3364–3367.

[29] P. Zhao, In situ FTIR-attenuated total reflection spectroscopic investigations on the base-acid transitions of polyaniline. Base-acid transition in the emeraldine form of polyaniline, J. Chem. Soc., Faraday Trans., 92 (1996) 3063–3067.

[30] S.S. Umare, B.H. Shambharkar, R.S. Ningthoujam, Synthesis and characterization of polyaniline–Fe_3O_4 nanocomposite: electrical conductivity, magnetic, electrochemical studies, Synth. Met., 160 (2010) 1815–1821.

[31] T. Abdiryim, X.G. Zhang, R. Jamal, Comparative studies of solid-state synthesized polyaniline doped with inorganic acids, Mater. Chem. Phys., 90 (2005) 367–372.

[32] S. Zhang, M. Zeng, W. Xu, J. Li, J. Li, J. Xu, X. Wang, Polyaniline nanorods dotted on graphene oxide nanosheets as a novel super adsorbent for Cr(VI), Dalton Trans., 42 (2013) 7854–7858.

[33] Z. Ying, H. Chen, L. Jie, C. Chen, Hierarchical MWCNTs/Fe_3O_4/PANI magnetic composite as adsorbent for methyl orange removal, J. Colloid Interface Sci., 450 (2015) 189–195.

[34] G. Annadurai, R.S. Juang, D.J. Lee, Use of cellulose-based wastes for adsorption of dyes from aqueous solutions, J. Hazard. Mater., 92 (2002) 263–274.

[35] S.K. Das, P. Ghosh, I. Ghosh, A.K. Guha, Adsorption of rhodamine B on *Rhizopus oryzae*: Role of functional groups and cell wall components, Colloids Surf., B, 65 (2008) 30–34.

[36] J.H. Huang, K.L. Huang, S.Q. Liu, A.T. Wang, C. Yan, Adsorption of Rhodamine B and methyl orange on a hypercross-linked polymeric adsorbent in aqueous solution, Colloids Surf., A, 330 (2008) 55–61.

[37] P.S. Kumar, S. Ramalingam, C. Senthamarai, M. Niranjanaa, P. Vijayalakshmi, S. Sivanesan, Adsorption of dye from aqueous solution by cashew nut shell: studies on equilibrium isotherm, kinetics and thermodynamics of interactions, Desalination, 261 (2010) 52–60.

[38] R. Ahmad, R. Kumar, Adsorption of Amaranth dye onto alumina reinforced polystyrene, Clean, 39 (2011) 74–82.

[39] Y.-F. Pan, C.T. Chiou, T.-F. Lin, Adsorption of arsenic(V) by iron-oxide-coated diatomite (IOCD), Environ. Sci. Pollut. Res., 17 (2010) 1401–1410.

[40] K.P. Singh, D. Mohan, S. Sinha, G.S. Tondon, D. Gosh, Color removal from wastewater using low-cost activated carbon derived from agricultural waste material, Ind. Eng. Chem. Res., 42 (2003) 1965–1976.

[41] F. Lux, Properties of electronically conductive polyaniline: a comparison between well-known literature data and some recent experimental findings, Polymer, 35 (1994) 2915–2936.

[42] V. Shaktawat, N.S. Saxena, K. Sharma, Study of the structure and mechanical properties of pure and doped polyaniline, Phase Transitions, 84 (2011) 215–224.

Supporting information

S1. Adsorption kinetics of RhB

It can be seen that at all studied initial dye concentrations, the straight lines with high correlation coefficients (≥0.991) were obtained, as seen in Fig. S1 and Table S1. The results suggest that the adsorption of RhB onto PANI@iron oxide is governed by pseudo-second-order rate kinetics.

S2. Adsorption isotherms of RhB

Compared the correlation coefficients of three models in Fig. S2 and Table S2, it was concluded that the Freundlich isotherm model was precisely fit the equilibrium data at temperature ranging from 298 to 328 K. And the value of n in Freundlich isotherm was greater than 1, which indicates that the RhB is favorably adsorbed onto PANI@iron oxide.

S3. Adsorption thermodynamics of RhB

The thermodynamic parameters for the adsorption of RhB are calculated and shown in Fig. S3 and Table S3. The positive value of $\Delta H°$ shows that the adsorption of RhB on PANI@iron oxide is endothermic. The positive value of $\Delta S°$ reveals the increasing randomness at the solid–solution interface during the adsorption process. The values of $\Delta G°$ are negative and decrease with an increase in temperature, which indicate that the adsorption process is spontaneous.
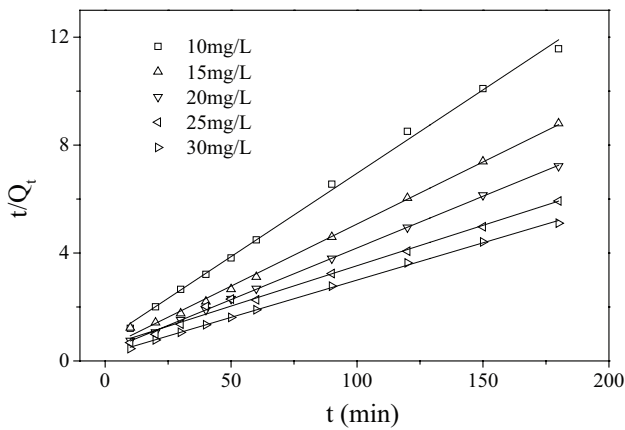
Fig. S1. Plots of t/Q_t vs. t at different initial RhB.

Table S1
Adsorption kinetic parameters of RhB

RhB (mg·L^{-1})	Q_e (mg·g^{-1})	k_2 (×10^{-3}) (g·mg^{-1}·min^{-1})	R^2
10	16.18	4.92	0.9971
15	21.72	4.95	0.9975
20	26.11	4.08	0.9998
25	33.42	2.65	0.9912
30	36.19	3.26	0.9989
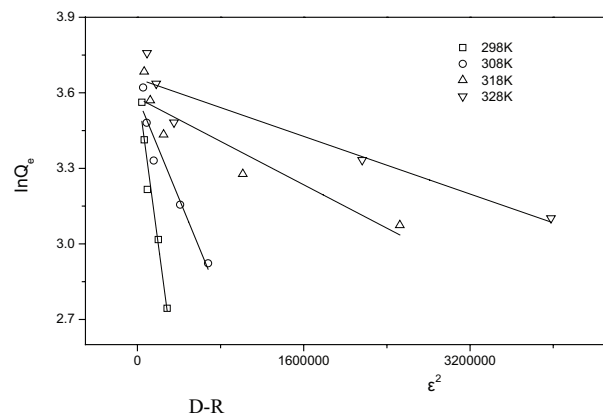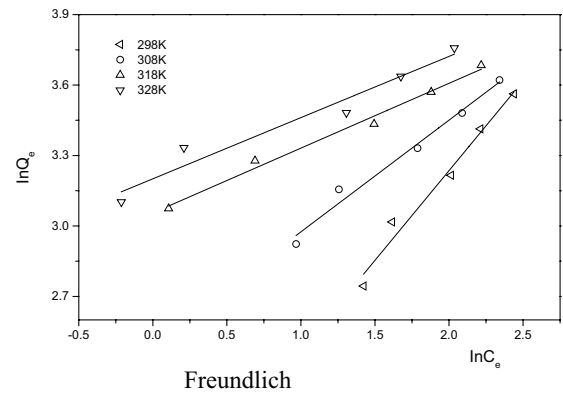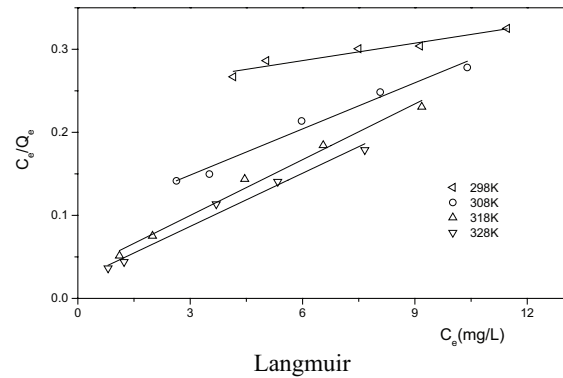
Fig. S2. Fitting plots for RhB adsorption based on isotherm models.

Table S2
Fitting parameters for RhB adsorption based on isotherm models

T (K)	Q (mg·g⁻¹) (experimental value)	Langmuir			Freundlich		D–R		
		K_L	R^2	K_F	R^2	n	K_{DR} (×10⁻⁶)	E (kJ·mol⁻¹)	R^2
298	35.26	0.0286	0.9128	5.515	0.9698	1.309	3.10	0.40	0.9443
308	37.38	0.1994	0.9758	12.18	0.9762	2.103	1.00	0.71	0.9176
318	39.81	0.6841	0.9848	21.23	0.9853	3.624	0.22	1.52	0.8206
328	42.85	0.9401	0.9778	24.55	0.9791	3.837	0.14	1.87	0.8541
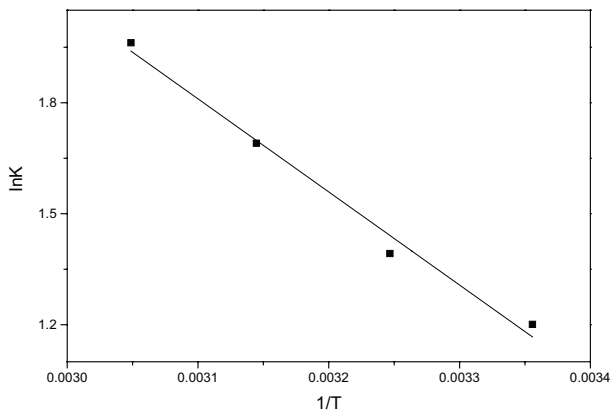
Fig. S3. Plots of ln$K$ vs. 1/T of RhB.

Table S3
Thermodynamic parameters for the adsorption of RhB at different temperatures

T (K)	K	$\Delta G°$ (kJ·mol⁻¹)	$\Delta S°$ (J·K⁻¹·mol⁻¹)	$\Delta H°$ (kJ·mol⁻¹)
298	3.33	−2.98	79.90	20.92
308	4.02	−3.45		
318	5.42	−4.19		
328	7.11	−4.86		